Measurement of the 238U(n, γ) cross section up to 80 keV with the Total Absorption Calorimeter at the CERN n_TOF facility

(n_TOF Collaboration) Wright, T.; ...; Bosnar, Damir; ...; Žugec, Petar

Measurement of the ^{238}U(n,γ) cross section up to 80 keV with the Total Absorption Calorimeter at the CERN n_TOF facility

T. Wright,[1,*] C. Guerrero,[2,3] J. Billowes,[1] D. Cano-Ott,[4] E. Mendoza,[4] S. Altstadt,[5] J. Andrzejewski,[6] L. Audouin,[7] V. Bécares,[4] M. Barbagallo,[8] F. Bečvář,[9] F. Belloni,[10] E. Berthoumieux,[10] D. Bosnar,[11] M. Brugger,[2] F. Calviño,[12] M. Calviani,[2] C. Carrapiço,[13] F. Cerutti,[2] E. Chiaveri,[2,10] M. Chin,[2] N. Colonna,[8] G. Cortés,[12] M. A. Cortés-Giraldo,[3] M. Diakaki,[14] M. Dietz,[15] C. Domingo-Pardo,[16] I. Durán,[17] N. Dzysiuk,[18] C. Eleftheriadis,[19] A. Ferrari,[2] K. Fraval,[10] V. Furman,[20] M. B. Gómez-Hornillos,[12] S. Ganesan,[21] A. R. García,[4] G. Giubrone,[16] I. F. Gonçalves,[13] E. González-Romero,[4] A. Goverdovski,[22] E. Griesmayer,[23] F. Gunsing,[10] P. Gurusamy,[21] T. Heftrich,[5] A. Hernández-Prieto,[2,12] D. G. Jenkins,[24] E. Jericha,[23] F. Käppeler,[25] Y. Kadi,[2] D. Karadimos,[14] T. Katabuchi,[26] V. Ketlerov,[22] V. Khryachkov,[22] P. Koehler,[27] M. Kokkoris,[14] J. Kroll,[9] M. Krtička,[9] C. Lampoudis,[10] C. Langer,[5] E. Leal-Cidoncha,[17] C. Lederer,[28] H. Leeb,[23] L. S. Leong,[7] J. Lerendegui-Marco,[3] R. Losito,[2] A. Manousos,[19] J. Marganiec,[6] T. Martínez,[4] C. Massimi,[29,30] P. Mastinu,[18] A. Mengoni,[31] P. M. Milazzo,[32] F. Mingrone,[29] M. Mirea,[33] C. Paradela,[17] A. Pavlik,[28] J. Perkowski,[6] J. Praena,[34] J. M. Quesada,[3] T. Rauscher,[35] R. Reifarth,[5] A. Riego-Perez,[12] M. Robles,[17] F. Roman,[33] C. Rubbia,[2] J. A. Ryan,[1] M. Sabaté-Gilarte,[2,3] R. Sarmento,[13] A. Saxena,[21] P. Schillebeeckx,[36] S. Schmidt,[5] D. Schumann,[37] P. Sedyshev,[20] G. Tagliente,[8] J. L. Tain,[16] A. Tarifeño-Saldivia,[16] D. Tarrío,[17] L. Tassan-Got,[7] A. Tsinganis,[2] S. Valenta,[9] G. Vannini,[29,30] V. Variale,[8] P. Vaz,[13] A. Ventura,[29] M. J. Vermeulen,[24] R. Versaci,[2] V. Vlachoudis,[2] R. Vlastou,[14] A. Wallner,[38] T. Ware,[1] M. Weigand,[5] C. Weiss,[23] and P. Žugec[11]

(The n_TOF Collaboration)

[1]*University of Manchester, United Kingdom*
[2]*European Organization for Nuclear Research (CERN), Switzerland*
[3]*Universidad de Sevilla, Spain*
[4]*Centro de Investigaciones Energéticas Medioambientales y Tecnológicas (CIEMAT), Spain*
[5]*Goethe University Frankfurt, Germany*
[6]*University of Lodz, Poland*
[7]*Institut de Physique Nucléaire, CNRS-IN2P3, Université Paris-Sud, Université Paris-Saclay, F-91406 Orsay Cedex, France*
[8]*Istituto Nazionale di Fisica Nucleare, Sezione di Bari, Italy*
[9]*Charles University, Prague, Czech Republic*
[10]*CEA Irfu, Université Paris-Saclay, F-91191 Gif-sur-Yvette, France*
[11]*Department of Physics, Faculty of Science, University of Zagreb, Zagreb, Croatia*
[12]*Universitat Politècnica de Catalunya, Spain*
[13]*Instituto Superior Técnico, Lisbon, Portugal*
[14]*National Technical University of Athens, Greece*
[15]*School of Physics and Astronomy, University of Edinburgh, United Kingdom*
[16]*Instituto de Física Corpuscular, Universidad de Valencia, Spain*
[17]*University of Santiago de Compostela, Spain*
[18]*Istituto Nazionale di Fisica Nucleare, Sezione di Legnaro, Italy*
[19]*Aristotle University of Thessaloniki, Thessaloniki, Greece*
[20]*Joint Institute for Nuclear Research (JINR), Dubna, Russia*
[21]*Bhabha Atomic Research Centre (BARC), India*
[22]*Institute of Physics and Power Engineering (IPPE), Obninsk, Russia*
[23]*Technische Universität Wien, Austria*
[24]*University of York, United Kingdom*
[25]*Karlsruhe Institute of Technology, Campus North, IKP, 76021 Karlsruhe, Germany*
[26]*Tokyo Institute of Technology, Japan*
[27]*Oak Ridge National Laboratory (ORNL), Oak Ridge, Tennessee 37831, USA*
[28]*University of Vienna, Faculty of Physics, Vienna, Austria*
[29]*Istituto Nazionale di Fisica Nucleare, Sezione di Bologna, Italy*
[30]*Dipartimento di Fisica e Astronomia, Università di Bologna, Italy*
[31]*Agenzia nazionale per le nuove tecnologie (ENEA), Bologna, Italy*
[32]*Istituto Nazionale di Fisica Nucleare, Sezione di Trieste, Italy*
[33]*Horia Hulubei National Institute of Physics and Nuclear Engineering, Romania*
[34]*University of Granada, Spain*
[35]*Department of Physics, University of Basel, Switzerland*
[36]*European Commission, Joint Research Centre, Geel, Retieseweg 111, B-2440 Geel, Belgium*

[37] *Paul Scherrer Institut (PSI), Villingen, Switzerland*
[38] *Australian National University, Canberra, Australia*
(Received 24 August 2017; published 1 December 2017)

The radiative capture cross section of a highly pure (99.999%), 6.125(2) grams and $9.56(5)\times10^{-4}$ atoms/barn areal density ^{238}U sample has been measured with the Total Absorption Calorimeter (TAC) in the 185 m flight path at the CERN neutron time-of-flight facility n_TOF. This measurement is in response to the NEA High Priority Request list, which demands an accuracy in this cross section of less than 3% below 25 keV. These data have undergone careful background subtraction, with special care being given to the background originating from neutrons scattered by the ^{238}U sample. Pileup and dead-time effects have been corrected for. The measured cross section covers an energy range between 0.2 eV and 80 keV, with an accuracy that varies with neutron energy, being better than 4% below 25 keV and reaching at most 6% at higher energies.

DOI: 10.1103/PhysRevC.96.064601

I. INTRODUCTION AND MOTIVATION

Nuclear energy is an unavoidable component of future energy production, as outlined in the EU SET plan [1]. In order to improve the sustainability of this energy source, new concepts for nuclear systems are being explored. In this context, despite many previous measurements, challenges still exist within the present level of basic nuclear data knowledge, as is shown in the case of ^{238}U. Recent efforts by the Collaborative International Evaluated Library Organization (CIELO) [2] have been made to evaluate the ^{238}U(n,γ) reaction [2] in the epithermal energy region. Thus it is timely to provide new data sets using modern, sophisticated detection and analysis techniques and tools.

There is indeed a requirement from industry to reduce the uncertainty in the ^{238}U(n,γ) cross section, as stated in the WPEC-26 report [3], which forms the basis for an entry in the OECD NEA High Priority Request List [4]. Here is stated the need for a reduction in the uncertainty of the ^{238}U(n,γ) cross section in particular neutron energy regions where the target uncertainty is lower than the current. Three energy regions are distinguished: 22.6–454 eV (currently 2%, required 1%), 2.03–9.12 keV (currently 3%, required 1%), and 9.12–24.8 keV (currently 9%, required 3%).

These energy regions essentially cover the resolved resonance region (RRR), which is currently described by a set of resonance parameters up to 20 keV. It has been demonstrated that the uncertainty in k_{eff} calculations propagated by the ^{238}U(n,γ) cross section is sensitive to individual resonance parameters [5] therefore there is a clear need for a reduction in uncertainty.

The latest evaluation in 2005 of the nuclear data available on ^{238}U(n,γ) by Derrien *et al.* [6,7] aimed to address and quantify the situation and these results have been mostly adopted by the three main neutron cross-section libraries (ENDF/B, JEFF, and JENDL). These libraries have an uncertainty in the capture cross section of 2–3% in the energy region from 100 eV–5 keV, however, Derrien *et al.* highlighted sizable differences (10%) between the different high-accuracy data sets.

A new measurement performed with the Total Absorption Calorimeter at the state of the art neutron time-of-flight facility n_TOF is described in detail, with particular attention to the experimental and analytical aspects. This paper focuses on the energy region from 0.2 eV–80 keV, spanning the resolved resonance region and part of the unresolved resonance region.

A single measurement is not sufficient to reach the desired accuracies for this cross section therefore an international combined effort has been made to acquire new data. The measurement discussed herein is a result of the EC-FP7 ANDES project [8] at the neutron time-of-flight facilities, n_TOF and GELINA [9], where measurements were performed with C_6D_6 liquid scintillators, details of which can be found in references [10,11]. By combining the new data sets, the next evaluation should be able to reach the required accuracies for advanced nuclear systems.

II. CURRENT DATA

The current high-quality capture data sets in the resonance region are from Moxon [12], de Saussure *et al.* [13], and Macklin *et al.* [14], which have all been previously analyzed in parallel with transmission data [6]. The important details from these three measurements are

(i) Moxon: Cross section measured with a Moxon Rae detector [15] on a 32.57 m flight path at the Harwell 45 MeV electron linear accelerator using 99.965% enriched 1.595×10^{-3} atoms/barn sample with normalization to the then accepted resonance parameters between 6 eV and 1 keV, the first three of which were saturated resonances.

(ii) de Saussure *et al.*: Cross section measured with the ORELA liquid scintillator tank (ORELAST) [16] on a 40 m flight path at ORELA [17] using two 99.99% enriched samples of 2.83×10^{-3} and 3.96×10^{-4} atoms/barn thicknesses. Normalization was made to the first (6.67 eV) resonance using the saturated resonance technique [18].

(iii) Macklin *et al.*: Cross section measured with ORELAST on a 150 m flight path at ORELA using two 99.99% enriched samples of thicknesses 3.09×10^{-3} and 1.236×10^{-2} atoms/barn with the normalization

*Corresponding author: tobias.wright@manchester.ac.uk

calculated from eight isolated small resonances in the region 600–1100 eV.

The status of the evaluated data files for ^{238}U in the resonance region is summarized in Ref. [19]. In summary, in order for these data sets to be compatible with transmission data [20], additional backgrounds and energy-dependent normalization factors had to be implemented by the evaluators. Above the 6.67 eV resonance, the data of de Saussure *et al.* were renormalized by a factor of ∼0.9 and the data of Macklin by a factor of ∼1.1. A further neutron energy-dependent background subtraction of ∼10% was required for both data sets. It is noted that these capture data sets included in the most recent evaluations had to be renormalized by sizable factors and that these factors are not even constant in energy. One could conclude these capture experiments have suffered from large (8–13%) uncertainties due to systematic effects. Indeed, discrepancies within these data sets limit the accuracy of the evaluated ^{238}U(n,γ) cross section.

Besides the recent GELINA and n_TOF measurements, a new cross-section measurement in the energy range 10 eV–500 keV has been reported using the DANCE calorimeter at the LANSCE facility [21]. Finally, due to the large amount of data sets available, the ^{238}U(n,γ) cross section was recently evaluated by Carlson *et al.* [22].

III. EXPERIMENTAL SET UP

A. n_TOF facility

The n_TOF facility is a pulsed neutron spallation source driven by 20 GeV/c protons, supplied by the CERN Proton Synchrotron, impinging on a cylindrical (40 cm length and 60 cm diameter) lead target. The ∼300 neutrons emitted by each proton initially have a fast neutron energy spectrum, which is moderated by a 4 cm layer of water and a further 1 cm of borated water in the horizontal plane, the former also acting as a coolant to the target. Two beam lines are used at n_TOF: one 185 m horizontal flight path leading to experimental area one (EAR1) and one 20 m vertical flight path leading to experimental area two (EAR2). The 185 m flight path offers excellent neutron energy resolution and therefore is well suited for a high-precision measurement of the ^{238}U resonance region. For neutron capture measurements at n_TOF, two detection systems are habitually used, utilizing the total energy and total absorption techniques. For the former, low-efficiency liquid scintillators (C_6D_6) detectors are used in combination with the pulse height weighting technique [23] and for the latter a 4π array of BaF_2 detectors is utilized. This paper deals with the analysis and results from the total absorption technique, where the goal is to analyze all the BaF_2 modules in coincidence in order to unambiguously detect a capture cascade. The neutron beam is monitored by the silicon monitor (SiMon) [24] where α and triton particles from the standard cross section ^{6}Li(n,α)^{3}H are detected. For a detailed description of the n_TOF facility and EAR1 see Ref. [25].

B. TAC detector

The Total Absorption Calorimeter (TAC) [26] is a segmented array of 40 BaF_2 crystals designed to detect the complete γ-ray cascade emitted during a neutron capture reaction. Based on a previous BaF_2 calorimeter at FZK [27], the 95% solid angle coverage allows capture cascades to be detected with an efficiency close to 100%. The 40 segments are composed of 12 pentagonal and 28 hexagonal BaF_2 crystals of 15 cm thickness, which fit together as a hollow sphere with an inner radius of 20 cm. Each individual crystal is surrounded by two layers of 0.1 mm thick Teflon foil and a 0.1 mm thick polished aluminium sheet to optimize light collection. Furthermore, the crystals are encased by a protective layer of ^{10}B enriched carbon fiber, which has the purpose of absorbing neutrons so they do not reach the crystals. The crystals are all supported by an aluminium honeycomb structure, which is split into two hemispheres that can be separated allowing access to the center of the TAC.

In order to minimize the probability of detecting neutrons scattered in the sample and subsequently being captured in the TAC, the hollow space between the sample and the BaF_2 crystals is filled with a borated polyethylene (enriched to 5% of ^{10}B) neutron absorber [28].

Each crystal's signal is fed into a single channel of a high performance digitizer (Acquiris-DC270) with 8-bit resolution, 8 MB memory, and 250 MHz sampling rate. This allows data to be recorded for 32 ms, which corresponds to the time-of-flight for 0.2 eV neutrons. The digitized waveforms are transferred via gigabit ethernet to the Cern advanced storage manager (CASTOR), where they are stored on both disk and tape for offline analysis.

The TAC heavily suffers from the γ flash [25], a short burst of relativistic particles traveling through the beam line and arriving to the experimental setup before the fastest neutrons. The time it takes to recover from the γ flash gives an upper limit in neutron energy for measurements with the TAC of a few keV with the nominal intensity n_TOF beam [7×10^{12} protons per pulse (ppp)]. Since the aim was to reach several tens of keV in this measurement, the proton beam was operated at lower intensities: 1.0 and 0.5×10^{12} ppp (referred to as HIGH and LOW respectively), which allowed neutron energies of 30 and 80 keV to be reached, respectively. An advantage of running with different beam intensities is that it provides results with different counting rates, which allows a check of both the effect and validity of count rate variable data corrections; such as pileup and dead-time.

C. Samples

The ^{238}U target, provided by EC-JRC-Geel, weighs 6.125(2) grams [$9.56(5)\times10^{-4}$ atoms/barn] and has a purity of 99.999%, with traces of ^{234}U (<1 ppm), ^{235}U (∼11 ppm) and ^{236}U (<1 ppm). The weight was confirmed at CERN upon reception of the target. Its rectangular (53.90×30.30 mm^2) shape covers 97% of the n_TOF neutron beam. In order to comply with radioprotection regulations, the sample was encased in ∼60 μm of aluminium and ∼75 μm Kapton. Targets with the same geometry made of gold [1.561(2) g] and carbon [14.638(2) g] were measured under similar conditions for validation and neutron scattering background studies, respectively.

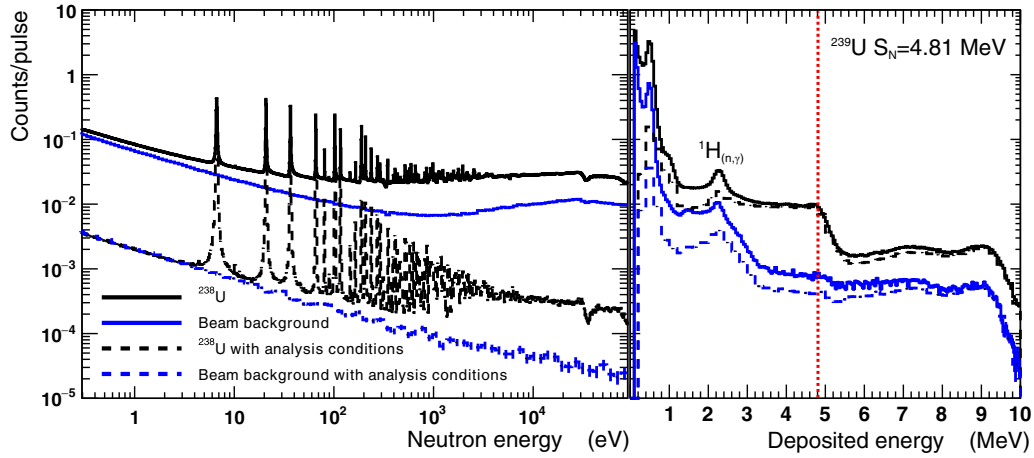

FIG. 1. Raw counts per histogram bin with and without the ^{238}U sample in place per pulse as a function of neutron energy (left) and deposited energy (in the neutron energy range 1–10 keV) (right) compared to counts with analysis conditions of $m_{cr} > 1$ and $2.5 < E_{sum}(\text{MeV}) < 5.75$. The dip at 30 keV neutron energy is due to neutrons interacting with aluminium in the beam line and the structures in the deposited energy spectra correspond to neutron capture reactions with the sample plus surrounding materials.

IV. ^{238}U CAPTURE YIELD

The observable quantity in a time-of-flight capture cross-section measurement is the experimental yield $[Y(E_n)]$, defined as the number of reactions per incident neutron. To arrive at this quantity, the initial data must first be reduced, before backgrounds are subtracted and any further corrections are made, as is detailed within this section.

A. Data reduction

The digitized BaF_2 signals are processed with a dedicated pulse shape analysis routine [29]. Each γ-ray signal has a fast and slow scintillation component. The background from the intrinsic α decay of the radium impurities in the crystals is eliminated from the final data analysis as the signals originating from α particles lack a fast component, however, was used for gain monitoring during the experimental campaign. During the measurement, which lasted 35 days, weekly calibrations were performed using standard γ-ray sources of ^{137}Cs (662 keV), ^{88}Y (898 and 1836 keV), and AmBe (4438 keV).

The target to sample neutron flight path L (185.61 ± 0.02 m) was determined by fitting 20 resonances in the ^{238}U data below 1 keV and calibrating to the accurately known resonance energies in the JEFF 3.1.2 evaluation.

The 40 digitizer channels were synchronized in time using a ^{88}Y calibration source. The signals from all individual detectors are then grouped into TAC events using a coincidence window of 20 ns after the first signal. Each TAC event is characterized by its time-of-flight (that of the first signal in the event), the sum energy of all the signals involved (deposited energy E_{sum}), and the number of BaF_2 crystals involved in the event (multiplicity m_{cr}). The reasonable energy resolution, high segmentation, and high absorption efficiency of the TAC allows identifying and rejecting background events by applying analysis conditions in m_{cr} and E_{sum}, see Ref. [26] for a detailed discussion. For this analysis, only events of multiplicities greater than one and energies between 2.5 and 5.75 MeV were used, eliminating at low γ-ray energies various backgrounds, particularly from ^{1}H(n,γ), and at high energies counts above the neutron separation energy of ^{239}U, which is 4.8 MeV, but a margin must be given due to small pileup events and detector resolution. As shown in Fig. 1, applying this condition helps improve the capture to background ratio by a factor of more than 15 in some resonances and $\sim$4 in the smooth keV region with a loss of $\sim$33% in efficiency.

B. Background subtraction

Many γ rays are detected in the crystals of the TAC originating from reactions other than neutron capture in ^{238}U, all contributing to a measured background. The main background components originate from a time-independent room background (beam-off), a time-dependent background from the neutron beam (sample-out), and background counts originating from other neutron reactions with the sample itself, predominantly neutron scattering. For this work, any background originating from fission events and in-beam γ rays scattered by the sample have not been considered and assumed to be negligible for the chosen analysis conditions.

The background due to the combination of the neutron beam and beam-off can be visualized through the counts as a function of time-of-flight and/or neutron energy or the deposited energy within the TAC (Fig. 1).

The time-independent background originates from natural radioactive sources present in the n_TOF measuring station, predominantly: ^{40}K found in the concrete walls, ^{238}U and its decay chain, and radium impurities and their decay chains within the BaF_2 crystals. Beam-off measurements throughout the experimental campaign totalling to around one day of running time were used to quantify this background, which, constant in time, follows the form $\frac{a}{\sqrt{E_n}}$ when expressed as a function of neutron energy. In order to reduce statistical fluctuations a fit of this form is performed to the experimental data before the background is subtracted.

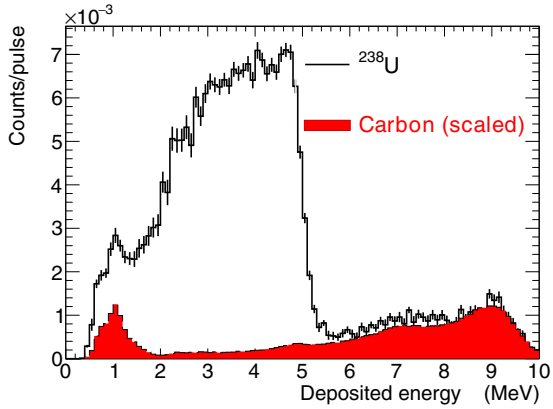

FIG. 2. Carbon and ^{238}U deposited energy spectra, per histogram bin, for $m_{cr} > 1$ and with the sample-out and beam-off backgrounds subtracted, where the carbon spectrum has been scaled above 7 MeV to match the number of ^{238}U counts to allow an estimation of the scattering contribution to the ^{238}U data.

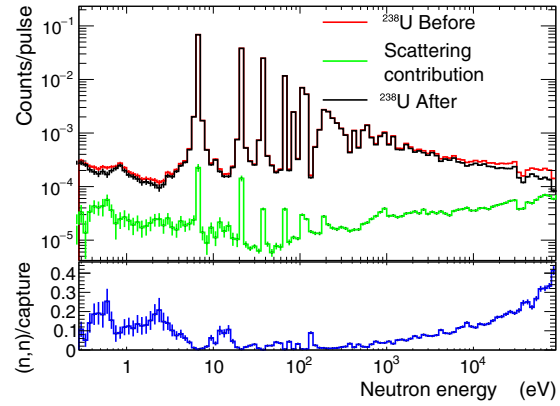

FIG. 3. Neutron scattering contribution to the ^{238}U data with 20 bins per decade.

The background originating from the neutron beam has two components: first, unrelated to the sample, determined with sample-out measurements, and second, counts caused by sample-scattered neutrons being captured elsewhere. The number of detected counts from scattered neutrons is heavily dependent on the ^{238}U(n,n) cross section, which has similar resonant structure as the ^{238}U(n,γ) cross section. This background is determined experimentally making use of the difference between the neutron separation energies of ^{239}U (4.8 MeV) and the barium isotopes present in the crystals (between 4.7 and 9.1 MeV). When neutrons are captured in the TAC crystals, γ-ray cascades can be emitted with a higher total energy than possible from a ^{238}U capture reaction, thus we assume that TAC events above a certain energy (7 MeV) originate from scattered neutrons. To then deduce the number of counts that will have been detected within the deposited energy cuts used in this work, $[2.5 < E_{sum}(\text{MeV}) < 5.75]$, the known scattered counts are compared to the carbon deposited energy spectrum, which is assumed to be a pure neutron scatterer. Thus, as shown in Fig. 2, by scaling the counts >7 MeV in the carbon data as a function of neutron energy to the ^{238}U deposited energy spectra, the background is estimated for the whole neutron energy region. A small percentage of the γ rays detected with energies above 7 MeV will not be from neutron capture on the barium isotopes but be due to pileup, hence an uncertainty is associated with this technique. The integral of the counts above 7 MeV from ^{238}U and ^{nat}C appear not to be equal in Fig. 2 as the full range of energies used for scaling (7–20 MeV) is not visible and the fractional pileup contribution to the two spectra in this energy region is different.

The magnitude of the correction from carbon scaling can be estimated analytically using the approximate efficiencies of the TAC to detect capture cascades $[\varepsilon_{n,\gamma}(m_{cr}, E_{sum})]$ and scattered neutrons $[\varepsilon_{n,n}(m_{cr}, E_{sum})]$. The former is measured with the saturated resonance technique and the latter is calculated by comparing the measured carbon yield with the theoretical carbon yield as given by SAMMY using the JEFF 3.1.2 carbon cross section. Knowing these and taking the capture and scattering resonance parameters from JEFF 3.1.2 (Γ_γ and Γ_n) we can estimate the neutron scattering contribution on a resonance-by-resonance basis. For example, following this method, the 36 eV resonance is expected to have a contribution from scattered neutrons of 0.8%, which is in perfect agreement with what is measured with the method of scaling to the carbon data. However, for higher-energy resonances, the analytical method breaks down as the time it takes a scattered neutron to be captured within the TAC is of the order a few hundred ns, which moves the subsequent capture time-of-flight outside the resonance.

The magnitude of the correction over the full neutron energy range is shown in Fig. 3. It is observed that as neutron energy increases, the contribution also increases as expected. This is mainly due to the ratio of capture to scattering cross sections for ^{238}U decreasing. Below 10 keV neutron energy, the correction is at most ~12%, rising to a maximum of 45% at 80 keV. Therefore it follows that if a 10% uncertainty is assigned to the subtraction method, no more than a 5% uncertainty is propagated to the final data.

C. Pileup and dead-time correction

The combination of the large sample, the high efficiency of the TAC and the intense pulsed neutron source at n_TOF-EAR1 (~10^6 neutrons per pulse) resulted in count rates as high as 1 count/μs in the peak of some resonances. The slow decay component of BaF_2 is ~630 ns, therefore pileup and dead time occur at these high count rates. The measured E_{sum} and m_{cr} of events are altered by these effects at high count rates pushing them outside or inside the chosen analysis conditions, thus introducing a complicated dependency of the detection efficiency on the count rate. To correct for this, a method has been developed for capture measurements with the TAC at the n_TOF facility [30].

To apply this method, TAC data has been analyzed to quantify the dead-time and pileup effect for two consecutive γ rays with energies E_1 and E_2 and at times t_1 and t_2. The value of the dead time varies with E_1 and E_2 between 0 and 3 μs and for this work, if $t_2 - t_1 < 250$ ns, pileup is assumed to occur and the two γ rays are assumed to be detected as one with an energy $E_1 + E_2$.

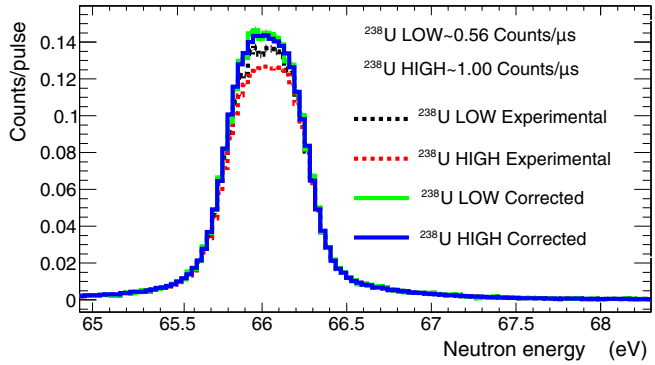

FIG. 4. The highest count rate in the data is found in the resonance at 66 eV. The asymmetrical resonance shape in the 1.0×10^{12} ppp (HIGH) data is removed after correcting for pileup and dead-time.

Data free from pileup and dead-time effects for the capture cascades in a region of low count rate is required as an input for this method; in this case, the tails of the 6.7 eV resonance are used. These realistic TAC cascades, each composed by a number of signals with measured energy and crystal number are randomly sampled and redistributed in time according to the measured count rate. Using the identified values of dead time and probability of pileup, the number of γ rays that would be missed in the analysis can be estimated, thus providing a more accurate true count rate. Through an iterative process, the effects of dead time and pileup have been determined and the true count rate accurately calculated.

The relatively high dead time of up to 3 μs is comparable to the width in time-of-flight of resonances in the eV region for ^{238}U, therefore not only will a loss of counts occur with high count rates but also the shape of the resonance can be distorted, as illustrated in Fig. 4. The expected symmetrical shape that is predicted by SAMMY is restored after the correction is applied. The pileup and dead-time correction is negligible across most of the data except in the stronger resonances below 1 keV. In these resonances, the correction is at most 15%.

D. Yield calculation

The measured capture yield $Y_{E_n}(n,\gamma)$ is defined as the probability of neutron capture and is calculated using:

$$Y(E_n) = \frac{C(E_n) - B(E_n)}{\varepsilon \cdot F \cdot \phi_n(E_n)}, \quad (1)$$

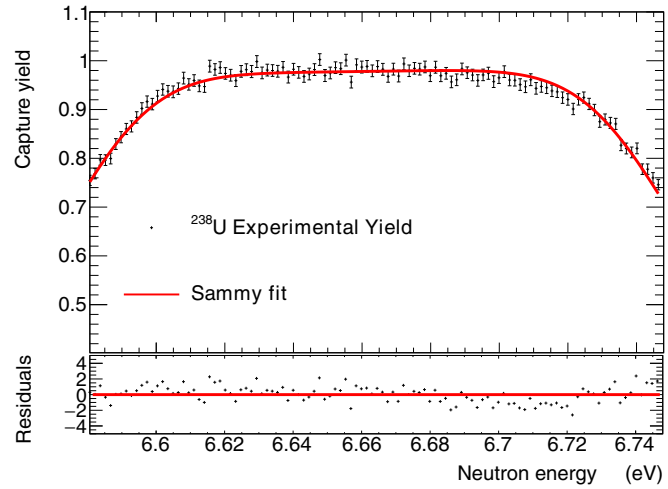

FIG. 5. The saturated peak of the first 6.7 eV ^{238}U resonance and residuals when compared to the SAMMY calculation.

where $C(E_n)$ and $B(E_n)$ are the total and background counts, respectively, ε is the efficiency for detecting capture cascades, F is the fraction of the beam intercepted by the ^{238}U target and $\phi_n(E_n)$ is the number of beam neutrons used in the measurement. The shape of the n_TOF neutron flux is known with an accuracy between 1% and 5% depending on the energy region, as specified in Table I. The product $\varepsilon \cdot F$ can be understood as a global normalization factor. In this particular experiment, the thickness of the ^{238}U target was chosen in such a way that the first three resonances are saturated, meaning that, at these resonance energies, almost all the neutrons incident on the target undergo at least one interaction, most more than one. This allows the saturated resonance method to be used to obtain an absolute normalization of the resulting capture yield. This is given by the corresponding comparison between the expected and measured yield at the saturated 6.7 eV resonance, where the expected resonance shape has been calculated by the SAMMY code [31] using the resonance parameters from the JEFF 3.1.2 library [32].

Figure 5 demonstrates the experimental yield scaled to the yield given by SAMMY for the first saturated resonance resulting in a scaling factor $\frac{1}{\varepsilon \cdot F}$ of 0.670 ± 0.007. The yield is scaled in the resonance peak only, where good agreement is found between the predicted yield by SAMMY and the

TABLE I. Summary of all the uncertainties except statistical related to the experimental ^{238}U capture yield.

Source of uncertainty	Uncertainty in energy range				
	<10 keV	10–25 keV	25–50 keV	50–60 keV	60–80 keV
Sample mass	0.03%				
Neutron flux	1–2%	2%	5%	2%	
Normalization	1%				
Dead-time and pileup	0–1%	Negligible			
Neutron scattering correction	0–2%	2%	2.5%	3%	4.5%
Beam-on and beam-off background	Negligible				
Residual background	0–2%	Negligible			
Overall	1.4–3.7%	3.0%	5.7%	3.7%	5.0%

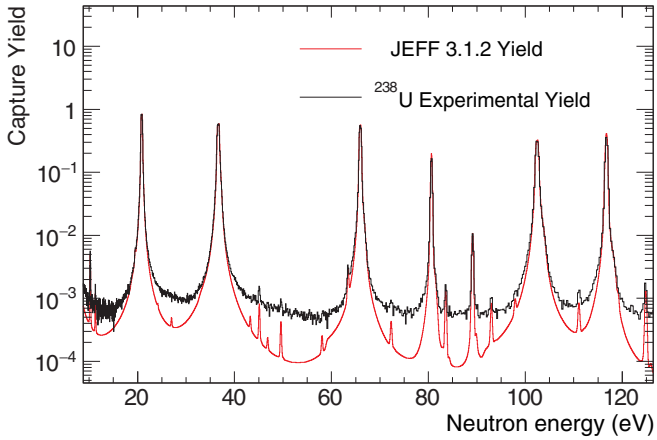

FIG. 6. The ^{238}U experimental yield after initial background subtraction compared to the calculated yield from SAMMY using resonance parameters from JEFF 3.1.2. A small background still remains within the data, which can be quantified by finding the required normalization to match the data to what is expected as a function of neutron energy.

experimental data. The accuracy of this technique for normalization is validated by the good agreement found in the second and third resonances, both of which are also saturated but not used for determining the normalization due to the larger multiple scattering corrections associated with these resonances, which incur an uncertainty into the resonance shape.

E. Residual background

After performing these background subtractions and finding the experimental yield, a residual background is observed similar to that seen in previous time-of-flight measurements, for example [33]. Figure 6 clearly shows the experimental yield still contains some background counts on a level only appreciable in the valleys between resonances, therefore any background contribution to the resonances themselves is negligible. This background can be determined as a function of neutron energy by comparing the measured and expected yields at the resonance valleys.

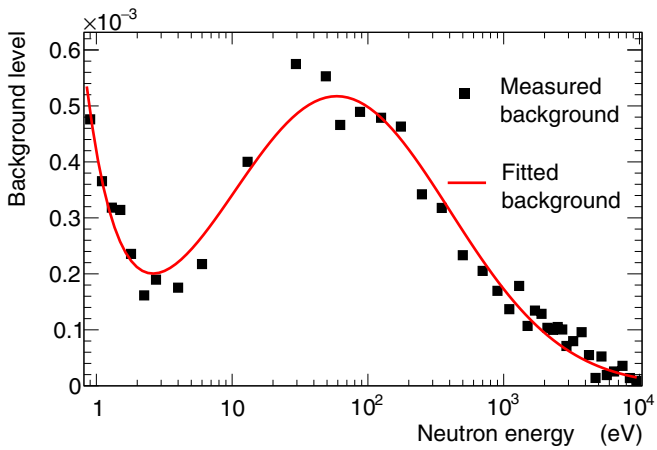

FIG. 7. Measured residual background points as a function of energy and the function found to best fit these data points.

This procedure has been performed at 41 points at various neutron energies up to 10 keV and it is observed in Fig. 7 that this background has clear structures on top of a $\frac{1}{v}$ dependence.

The background has a shape that can be analytically described by the function $BG(E_n) = a.e^{b.\log(E_n(eV))} + c.e^{\frac{E_n(eV)-d}{f}}$ with $a = 3.660\text{x}10^{-4}$, $b = -1.809$, $c = 5.203\text{x}10^{-4}$, $d = 4.081$, and $f = 1.909$. A capture yield should by definition be free from any backgrounds therefore these data have been provided in EXFOR [34,35] with and without this background subtracted. The method for quantifying this background is fully dependent on the set of resonance parameters chosen to produce the predicted yield from SAMMY, therefore it must be noted that where this background has a significant contribution to the measured counts, these data should be used with caution due to the dependence of the final yield on the resonance parameters chosen to calculate this background.

Figure 8 summarizes the individual and total background contributions to the data. Below 1 keV where there are strong and easily resolved resonances the data is dominated by counts from ^{238}U capture reactions, however, the residual background is on a level comparable to some resonance tails, therefore it can affect the resonance shapes. Thus, these data should be used with caution for resonance analysis below 1 keV due to the reliance on the evaluated cross section to determine this background. Compared to true ^{238}U capture counts, above 1 keV, the total background is ~40%, rising to ~50% between 40 and 60 keV and finally ~70% between 60 and 80 keV.

F. Discussion on uncertainties

The sources of uncertainty during the calculation of the experimental capture yield are related to the various backgrounds present (beam-off, beam-on, neutron scattering, and residual), the dead-time and pileup correction, the sample mass, and the neutron flux. The magnitude of these uncertainties varies as a function of neutron energy and is given in Table I. The background from scattered neutrons was subtracted by scaling the deposited energy data >7 MeV to the carbon spectra ignoring any pileup effects, which will change as a function of neutron energy. Due to this and also poor statistics in the deposited energy spectra in the >7 MeV region, a 10% uncertainty has been estimated for this background subtraction. Since the magnitude of the residual background can be well estimated and fitted, the uncertainty for this correction has also been estimated to be 10%. It is noted that the main contributors to the overall uncertainties are the neutron flux, particularly in the region 25–50 keV (due to aluminium in the beam line) and the correction for scattered neutrons. These total final uncertainties are comparable to the complementary n_TOF C_6D_6 measurement, which has a final uncertainty of between 2% and 6% in the same neutron energy ranges. The data from GELINA are reported with a lower uncertainty of 1.5%.

V. RESULTS

A. Resolved resonance region

Due to the long flight path and reasonable statistics acquired, individual resonances are resolved and analyzed (fitted) up to 5 keV neutron energy with a bin size $\frac{dE}{E}$ of

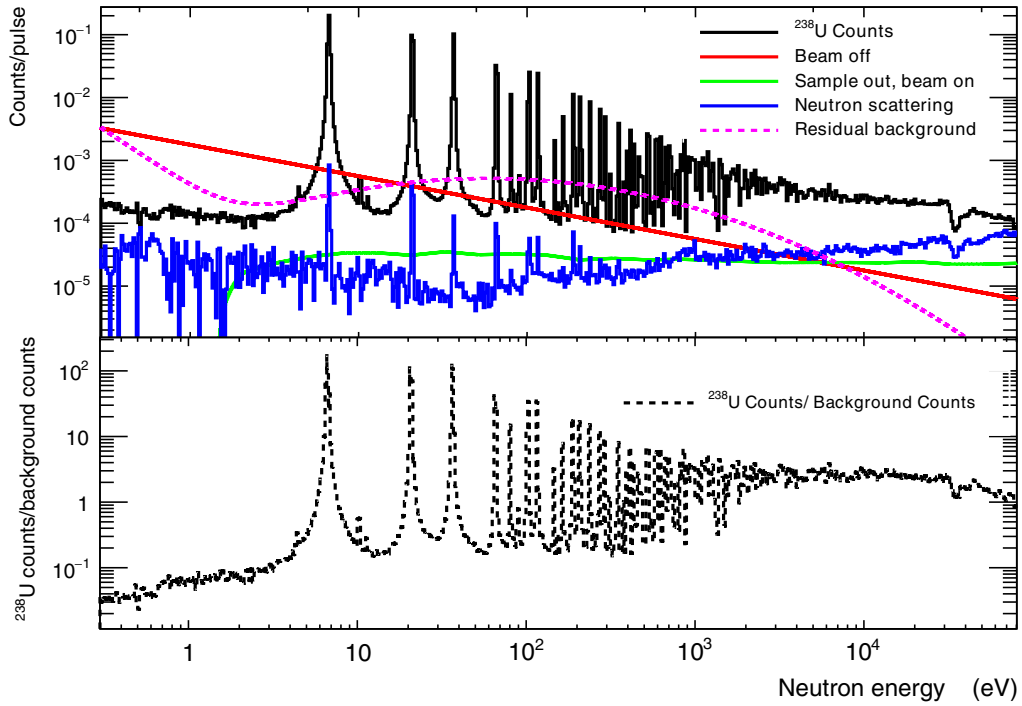

FIG. 8. Background subtracted ^{238}U counts are compared to the individual and total background contributions.

10^{-4}. In this region, the cross section is represented by a set of resonance parameters. In this case, to find these the R-matrix code SAMMY was used, leaving both the capture (Γ_γ) and neutron scattering (Γ_n) widths to vary as free parameters. The background component was also left to vary in line with the background associated uncertainties.

Figure 9 shows examples of the data and SAMMY fits from 4.5 keV–5 keV, which correspond to the upper limit in neutron energy it was possible to perform a resonance analysis for in this work due to statistical and background constraints.

Due to the high correlation between the resonance parameters obtained from a single data set it does not make sense to directly compare these values with others, therefore the comparison with evaluations is made using the resonance strength. This is calculated as the radiative kernel:

$$K_\gamma = g_j \cdot \frac{\Gamma_n \cdot \Gamma_\gamma}{\Gamma_n + \Gamma_\gamma}, \tag{2}$$

with the spin factor g_j defined as:

$$g_j = \frac{2J+1}{(2i+1)(2I+1)}, \tag{3}$$

where i, I, and J are spins of the incident particle, target nucleus (^{238}U: $I = 0^+$), and compound nucleus (^{239}U) respectively. Figure 10 shows the distribution of ratios for the radiative kernels obtained in this work compared to those from the JEFF 3.1.2 evaluation (equal to ENDF/B-VII.1 and JENDL-4.0 above 1 keV and almost identical below) and the

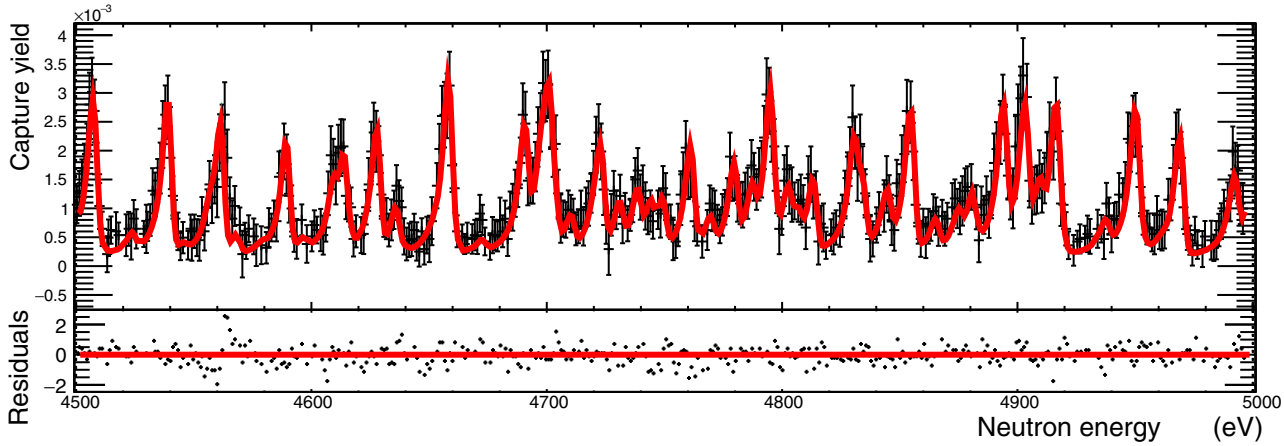

FIG. 9. Experimental capture yield (black) and the SAMMY fit (red) in the neutron energy interval 4.5–5 keV, which represents the statistical upper limit of possible resonance analysis. The resonance parameters and resonance kernels can be found in the EXFOR entry [35]

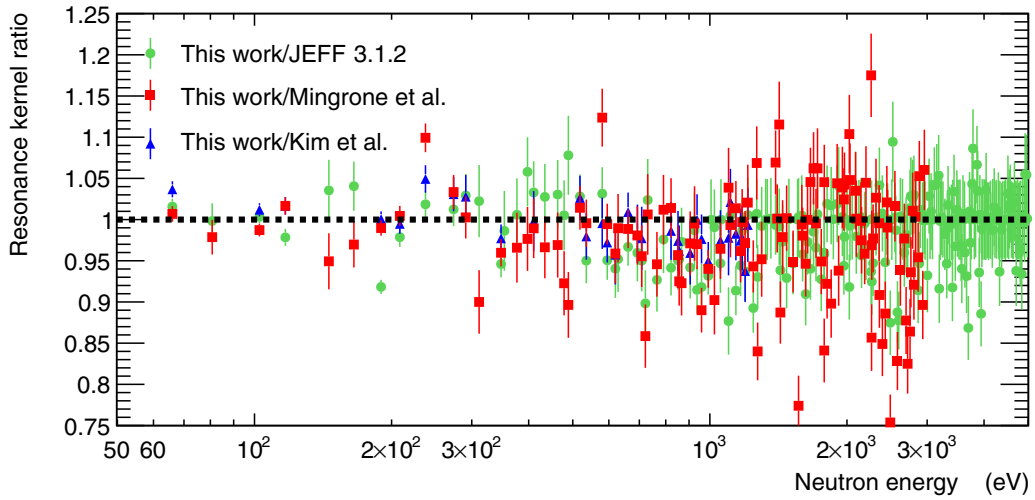

FIG. 10. Ratios of the capture resonance kernels determined from this work divided by those found by Mingrone *et al.* [10] and Kim *et al.* [11] and the JEFF 3.1.2 evaluation.

recent data of Mingrone *et al.* and Kim *et al.* On average, the data from this work is in good agreement with other data but in general the capture resonance kernel is slightly higher (1.3, 2.0 and 0.9% higher for JEFF 3.1.2, Mingrone *et al.,* and Kim *et al.,* respectively).

It is possible for uncertainties due to systematic effects to be present in capture experiments from such things as multiple scattering, pileup, and neutron scattering corrections. By looking only to stronger or weaker resonances, these corrections are larger or smaller, respectively. In the case of the TAC, for the 174 resonances with a resonance kernel $<$20 meV, excellent agreement is seen with the evaluated libraries (the distribution of kernel ratios has a Gaussian fit with a mean of 0.996 and $\sigma = 0.035$). However, for the 58 stronger resonances with a kernel $>$20 meV, TAC data are on average 4% below the evaluated data (the resulting Gaussian fit with a mean of 0.962 and $\sigma = 0.053$). This suggests that there may be some systematic effect in the analysis of strong resonances in either the TAC data or in the data considered in the current evaluations.

Future evaluations such as CIELO can use data from a variety of sample thicknesses, neutron facilities, and experimental techniques, thus a new evaluated resonance analysis will rule out any systematic effects associated with stronger resonances.

B. Unresolved resonance region

Above 5 keV, the capture cross section $\sigma_{n,\gamma}$ is calculated by:

$$\sigma_{n,\gamma} = \frac{Y_{n,\gamma}}{n \cdot C_f}, \tag{4}$$

where C_f is a correction factor for sample-related effects such as self-shielding and multiple interaction events. This correction factor has been calculated for the sample used during this experimental campaign using Monte Carlo simulations with MCNP [36] and GEANT4 [37] and has found to range between 2 and 5% (see [10] for more information). The measured average cross section is given along with uncertainties in Table II.

TABLE II. Average ^{238}U(n,γ) cross-section values and relative uncertainties. For a more detailed data set see the EXFOR entry [35].

Neutron energy (eV)	Cross section (b)		Relative uncertainties (%)	
	Value	Uncertainty	Systematic	Statistical
1000–1500	2.01	0.07	3.7	0.0003
1500–2000	1.64	0.06	3.7	0.0004
2000–2500	1.53	0.06	3.7	0.0005
2500–3000	1.28	0.05	3.7	0.0006
3000–3500	1.33	0.05	3.7	0.0006
3500–4000	1.06	0.04	3.7	0.0008
4000–4500	0.88	0.03	3.7	0.001
4500–5000	0.98	0.04	3.7	0.0009
5000–5500	0.90	0.03	3.7	0.001
5500–6000	0.97	0.04	3.7	0.0011
6000–6500	0.98	0.04	3.7	0.0011
6500–7000	0.82	0.03	3.7	0.0012
7000–8000	0.80	0.03	3.7	0.001
8000–9000	0.67	0.02	3.7	0.0011
9000–10000	0.72	0.03	3.7	0.0011
10000–12000	0.68	0.02	3.0	0.0009
12000–14000	0.66	0.02	3.0	0.001
14000–16000	0.61	0.02	3.0	0.0011
16000–18000	0.59	0.02	3.0	0.0011
18000–20000	0.53	0.02	3.0	0.0014
20000–22500	0.53	0.02	3.0	0.0011
22500–25000	0.46	0.01	3.0	0.0015
25000–27500	0.47	0.03	5.7	0.0015
27500–30000	0.47	0.03	5.7	0.0016
30000–35000	0.46	0.03	5.7	0.0031
35000–40000	0.42	0.02	5.7	0.0041
40000–45000	0.40	0.02	5.7	0.0033
45000–50000	0.37	0.02	5.7	0.004
50000–60000	0.30	0.01	3.7	0.003
60000–70000	0.26	0.01	5.0	0.0037
70000–80000	0.22	0.01	5.0	0.0039

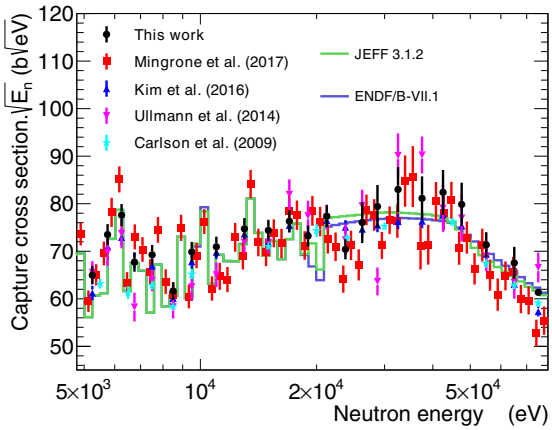

FIG. 11. Experimental ^{238}U(n,γ) cross section from this work compared to the other recent measurements and evaluations in the neutron energy range 5–80 keV.

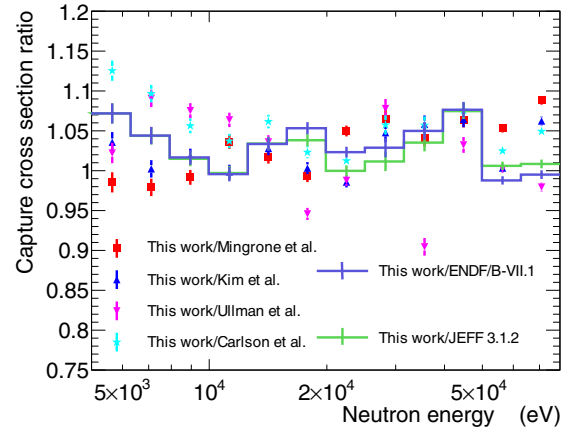

FIG. 12. Ratios of the measured ^{238}U(n,γ) cross section from this work and other recent measurements and evaluations.

The calculated TAC averaged cross section, with a $\frac{dE}{E} = 2 \times 10^{-2}$ binning is shown alongside the most recent measurements and evaluations in Fig. 11. In general reasonable agreement is found between all recent measurements and evaluations. In order to evaluate small differences between data sets, the cross-section ratios have been calculated and are shown in Fig. 12.

In the energy range 5–9 keV (current uncertainty 3%), the TAC data is in good agreement (1–2%) with the recent GELINA and n_TOF C_6D_6 measurements, but 4% higher than the evaluated libraries, 7% higher than the data from DANCE, and 8% higher than the Carlson evaluation. Between 9 and 25 keV (current uncertainty 9%), the data is on average 2–3% higher than the Carlson and library evaluations but in perfect agreement with the GELINA data and 1.5–2.5% higher than the DANCE and n_TOF C_6D_6 data sets, respectively. From 25–80 keV, the TAC data is on average in fair agreement with the evaluated libraries (1.5–2.5% higher) and 4–7% higher than the other measurements and the Carlson evaluation. The plethora of recent, accurate measurements confirm that the evaluations are correct within their rather large uncertainties (up to 9%), however, it is apparent that many data sets agree on a level of always better than 5% in the energy range up to 80 keV. A future cross-section evaluation through CIELO can certainly get closer to, if not meet, the required accuracy of 3% in these energy regions.

VI. CONCLUSIONS

The ^{238}U(n,γ) cross section has been measured with the Total Absorption Calorimeter (TAC) using the neutron time-of-flight technique at the CERN n_TOF facility. The resulting cross section covers the energy range between 0.2 eV and 80 keV with an accuracy ranging between 1.4% and 5.7%, depending on the energy range. The results of this work are in general slightly higher than current evaluations but in good agreement with other recent measurements, therefore it is expected that future evaluations will be modified to include these data sets. It is timely for a reevaluation of the ^{238}U(n,γ) cross section in order to best meet the required uncertainties for future reactors. In particular, in the neutron energy range between 9 and 25 keV, the current uncertainty is 9% but our data, along with the other measurements, show that the cross section can be reevaluated and constrained within an accuracy of at highest 5%, but most likely even better, reaching the required 3%.

ACKNOWLEDGMENTS

The authors acknowledge financial support from the UK Nuclear Decommissioning Authority (NDA), EPSRC, CERN, the EC-FP7 ANDES (FP7-249671) project, ENRESA under the CIEMAT-ENRESA agreement and the Spanish Ministry of Science and Innovation (FPA2005-06918-C03-01).

[1] *The European Strategic Energy Technology Plan (set-plan)* (European Commission).
[2] M. Chadwick *et al.*, Nucl. Data Sheets **118**, 1 (2014).
[3] NEA/WPEC-26, OECD Nuclear Energy Agency International Evaluation Co-operation, **26** (2008).
[4] https://www.oecd-nea.org/dbdata/hprl/.
[5] D. Rochman, A. Koning, and S. van der Marck, Ann. Nucl. Energy **36**, 810 (2009).
[6] H. Derrien, L. Leal, N. Larson, and A. Courcelle, ORNL/TM-2005/241 **019** (2005).
[7] H. Derrien, A. Courcelle, L. C. Leal, and N. M. Larson, Nucl. Sci. Eng. **161**, 131 (2009).
[8] A. Plompen *et al.*, Nucl. Data Sheets **119**, 201 (2014).
[9] A. Bensussan and J. Salome, Nucl. Instrum. Methods **155**, 11 (1978).
[10] F. Mingrone *et al.*, Phys. Rev. C **95**, 034604 (2017).
[11] H. I. Kim *et al.*, Eur. Phys. J. A **52**, 170 (2016).
[12] M. Moxon, Atomic Energy Research Establishment **6074**, (1967).
[13] G. de Saussure, E. G. Silver, R. B. Perez, R. Ingle, and H. Weaver, Nucl. Sci. Eng. **51**, 385 (1973).
[14] R. Macklin, R. Perez, G. de Saussure, and R. Ingle, Ann. Nucl. Energy **18**, 567 (1991).
[15] M. Moxon and E. Rae, Nucl. Instrum. Methods **24**, 445 (1963).

[16] F. C. Maienschein, (ORNL/TM-3833, 1972).
[17] K. Böckhoff, A. Carlson, O. Wasson, J. Harvey, and D. Larson, Nucl. Sci. Eng. **106**, 192 (1990).
[18] R. L. Macklin, J. Halperin, and R. R. Winters, Nucl. Instrum. Methods **164**, 213 (1979).
[19] S. Kopecky *et al.*, JRC Technical Report EUR 27504 EN, 2015.
[20] D. K. Olsen, G. de Saussure, R. B. Perez, E. G. Silver, F. C. Difilippo, R. W. Ingle, and H. Weaver, Nucl. Sci. Eng. **62**, 479 (1977).
[21] J. L. Ullmann, T. Kawano, T. A. Bredeweg, A. Couture, R. C. Haight, M. Jandel, J. M. ODonnell, R. S. Rundberg, D. J. Vieira, J. B. Wilhelmy, J. A. Becker, A. Chyzh, C. Y. Wu, B. Baramsai, G. E. Mitchell, and M. Krticka, Phys. Rev. C **89**, 034603 (2014).
[22] A. D. Carlson *et al.*, Nucl. Data Sheets **110**, 3215 (2009).
[23] A. Borella, G. Aerts, F. Gunsing, M. Moxon, P. Schillebeeckx, and R. Wynants, Nucl. Instrum. Methods A **577**, 626 (2007).
[24] S. Marrone *et al.*, Nucl. Instrum. Methods A **517**, 389 (2004).
[25] C. Guerrero *et al.*, Eur. Phys. J. A **49**, 27 (2013).
[26] C. Guerrero *et al.*, Nucl. Instrum. Methods A **608**, 424 (2009).
[27] K. Wisshak, K. Guber, F. Käppeler, J. Krisch, H. Müller, G. Rupp, and F. Voss, Nucl. Instrum. Methods A **292**, 595 (1990).
[28] E. Mendoza *et al.*, J. Kor. Phys. Soc. **59**, 1813 (2011).
[29] E. Berthoumieux, *Preliminary Report on* BaF_2 *Total Absorption Calorimeter Test Measurement*, Technical Report (CEA, 2004).
[30] C. Guerrero, D. Cano-Ott, E. Mendoza, and T. Wright, Nucl. Instrum. Methods A **777**, 63 (2015).
[31] N. M. Larson, ORNL/TM-9179/R8, ENDF-364/R2, 2008, 10.2172/941054.
[32] A. Koning *et al.*, J. Kor. Phys. Soc. **59**, 1057 (2011).
[33] C. Guerrero *et al.*, Phys. Rev. C **85**, 044616 (2012).
[34] N. Otuka *et al.*, Nucl. Data Sheets **120**, 272 (2014).
[35] http://www-nds.iaea.org/EXFOR/23364.
[36] T. Goorley *et al.*, Nucl. Tech. **180**, 298 (2012).
[37] S. Agostinelli *et al.*, Nucl. Instrum. Methods A **506**, 250 (2003).